Journal of Solid State Chemistry **149,** 320–326 (2000)
doi:10.1006/jssc.1999.8533, available online at http://www.idealibrary.com on IDEAL®

Chemical and Thermal Expansion of Calcium-Doped Lanthanum Chromite

R. E. Williford and T. R. Armstrong

Pacific Northwest National Laboratory, P.O. Box 999, Richland, Washington 99352

and

J. D. Gale

Department of Chemistry, Imperial College, South Kensington SW7 2AY, United Kingdom

Received August 10, 1999; in revised form October 6, 1999; accepted October 11, 1999

Atomistic free-energy minimization techniques were used to simulate three simultaneous volumetric shrinkage/expansion phenomena in calcium-doped lanthanum chromite solid oxide fuel cell (SOFC) interconnect materials. Four sets of interatomic potentials were developed and tested over the temperature range 0–1273 K. The predicted unit-cell volumes, elastic properties, volumetric shrinkage due to A-site doping of the ABO_3 perovskite $(La_{1-x}Ca_x)CrO_3$, defect-induced volumetric expansion due to reducing atmospheres, and thermal expansion were in reasonable agreement with experiment, though not all concurrently with a single set of potentials. Potentials based either on simple oxides or on partial charge models appeared to give the best overall predictions. Additional experimental data are needed to improve the potentials. © 2000 Academic Press

Key Words: **lanthanum chromite; calcium doping; coefficient of chemical expansion; coefficient of thermal expansion; atomistic models.**

1. INTRODUCTION

An operating solid oxide fuel cell (SOFC) has a chemical potential gradient between the air and fuel mixtures. The air and fuel are physically separated by a high-temperature ceramic interconnect material (acceptor-substituted lanthanum chromite), which must also maintain (a) high electronic conductivity, (b) a thermal expansion coefficient matched to the other stack components, and (c) mechanical integrity. These severe constraints must be satisfied at high temperatures and have generally limited the selection of interconnect materials for acceptor-substituted lanthanum chromites.

Under oxidizing conditions, electronic charge compensation occurs in acceptor-substituted lanthanum chromite by the formation of Cr^{4+} (1). However, when sufficiently reducing conditions prevail, oxygen vacancies form and the Cr^{4+} reduces to Cr^{3+} in order to maintain electrical neutrality via ionic compensation. The net result is a decrease in the electronic conductivity by a decrease in the number of charge carriers available to participate in small polaron hopping (2), a lattice expansion due to the change in the ionic radii of Cr (3, 4), and the development of an ionic conductivity due to oxygen vacancy formation (5, 6). The most important consequence of reducing environments in the present paper is the defect-induced lattice expansion, also called the coefficient of chemical expansion (CCE), because it strongly influences the mechanical integrity of the interconnect.

The defect-induced (or reduction-induced) CCE has been well documented for acceptor-substituted lanthanum and yttrium chromites (3, 4, 7–12). At 1273 K, the onset of expansion is between 10^{-10} and 10^{-12} atm O_2 for highly doped samples (>15 mol % acceptor), and nearly complete reduction of the tetravalent Cr occurs at 10^{-18} atm. The amount of expansion varies depending on which acceptor dopant is used and whether it occupies the A-site or the B-site in the ABO_3 perovskite lattice. For A-site substitution, lower expansions have been observed by doping with Sr rather than Ca. Mg is a favored dopant for B-site substitution because it typically results in lower expansions than Sr or Ca. However, this is not a fair comparison since additions to the B-site of both acceptors and donors have been shown to reduce the lattice expansion (3, 4, 7). It has been demonstrated that the amount of lattice expansion is proportional to the initial Cr^{4+} concentration in the sample, implying that the expansion is solely due to the increase in ionic radius associated with the reduction of Cr^{4+} to Cr^{3+} and is not due to interatomic repulsive forces arising from vacancy formation (3, 7).

0022-4596/00 $35.00

The use of ceramic interconnects has been limited at high temperatures due to defect-induced CCE and consequent failure of the interconnect. To date, the approach to developing new rare-earth chromite compositions with minimal expansion has been purely Edisonian in nature. Over the past decade, hundreds of compositions have been synthesized and tested at research institutions across the globe in order to find a suitable interconnect material. Composition development and testing still continues, and it is not certain whether a rare-earth chromite will be developed that meets *all* of the SOFC requirements.

The purpose of this study is to develop computational models that could eventually be used as design tools to predict the lattice expansion of rare earth chromites without the need for synthesizing and testing hundreds of compositions. The general technique used herein is called static lattice energy minimization. This approach is well founded in the literature, but as with all atomistic techniques, the results depend on how well the interatomic potentials describe the material. In our previous work on Sr-doped lanthanum chromites (13), development of the interatomic potentials was severely restricted in order to test the extrapolability of the general method in predicting SOFC material performance. This resulted in moderate underpredictions of the CCE dilations for reducing atmospheres. The present paper extends the energy minimization method to include volumetric shrinkage due to A-site substitutions and also thermal expansion for calcium-doped lanthanum chromites. Several sets of interatomic potentials are developed and tested, including one that treats partial covalency. Models are developed for $(La_{1-x}Ca_x)CrO_{3-\delta}$, and the results are compared to experimental data collected for samples with Ca concentrations ranging from $x = 0.20$ to $x = 0.30$.

2. EXPERIMENTAL MATERIALS AND DATA

All powders for this study were prepared by the glycine–nitrate process. The powder produced by the combustion event was passed through a 100-mesh screen, to break up large agglomerates, and then calcined at 1000°C for 1 h in air. The calcined powders were uniaxially pressed (55 MPa) into bars and then isostatically pressed at 138 MPa. The pressed compacts were sintered for 2 h in air at 1200 to 1700°C. Dilatometric measurements were used to determine the stability of synthesized chromites in highly reducing environments. The dilatometric experiments were carried out using sintered bars (30 mm × 3 mm × 3 mm) as a function of the ambient oxygen partial pressure ($P(O_2)$) using a buffered $CO_2/Ar/H_2$ gas system. The buffered gas system allowed measurements to be made over a $P(O_2)$ range from 10^{-5} to 10^{-18} atmospheres at 1000°C. More complete descriptions of the sample preparation are given in (3, 14).

For brevity of notation in the balance of the paper, the materials are described by the percentage of Ca substituted on the A-sites, i.e., 20% Ca is denoted LCC20 and 30% Ca is denoted LCC30. For the present paper, calculations were limited to the fully oxidized material (heated in air, denoted "ox") and the fully reduced material ($P(O_2) = 10^{-18}$ atm, denoted "red"). This study is also limited to the calcium-doped lanthanum chromites (LCC) because they appear more likely to retain the orthorhombic *Pbnm* symmetry at higher temperatures (3, 14), rather than transforming to rhombohedral symmetry as in the case of strontium doping (15). This simplified the potential derivations by reducing the amount of structural data needed. Such data are essentially nonexistent for the fully reduced cases at high temperatures.

Lattice parameters for the oxidized cases at 298 K were obtained from Table V of (3). Lattice parameters at 1273 K have not been measured. However, since reducing atmospheres cause the dilations that are of interest in this study, lattice parameters for the reduced cases were computed from those for the oxidized cases using the coefficient of chemical expansion (CCE) measured in recent experiments (see below). The reference unit-cell volumes were computed from these lattice constants. Stoichiometric coefficients for the reduced cases, i.e., $La_{1-x}Ca_xCr^{3+}_{1-x+2\delta}Cr^{4+}_{x-2\delta}O_{3-\delta}[V_O^{\cdot\cdot}]_\delta$, were obtained from Table III of (3) but corrected to read $\delta = 0.04$ and 0.06 for LCC20 and LCC30, respectively. Complete oxidation was assumed for the oxidized cases, because partial reduction based on Table III of (3) decreased the predicted CCE only by about 15–20%, so this is not a major factor. The Young's modulus (E) for these materials is about 180 GPa and is not sensitive to the $P(O_2)$ (16), so the bulk modulus $B = E/3(1 - 2\nu)$ is expected to be approximately 136 GPa, with Poisson's ratio taken as $\nu = 0.28$. The static dielectric constant cannot be reliably measured because these materials are good electronic conductors, but is expected to be very low. For the comparisons below, the experimentally measured CCE was 0.188 and 0.358% at 1273 K for LCC20 and LCC30, respectively (3, 14). No data were available for CCE at 0 K, so these same values were used because the thermal expansion is nearly the same for both cases. The experimentally measured A-site volume decrease (upon substitution of Ca) from LCC20 to LCC30 at 1273 K was −1.12% for the oxidized case and −0.21% for the reduced case (3). At 298 K, this volume decrease for the oxidized case was −1.08%, but no data were available for the reduced case at 298 K. The measured thermal expansion coefficient is 10.05–10.44 ppm/K (14) for both the oxidized and reduced cases.

3. COMPUTATIONAL METHODS

The appreciable ionic character of the bonding in lanthanum chromites ($La_{1-x}Ca_xCrO_3$) justifies the use of static

lattice energy minimization techniques in this investigation, largely employing formal charges and a shell model description of polarization. This technique has been successfully employed for the study of defect energetics in other perovskites (17–20). The General Utility Lattice Program (GULP) (21, 22) was used in this investigation to simulate the energetics and structures of $La_{1-x}Ca_xCrO_3$ on an atomistic scale. A Newton–Raphson energy minimization facility based on the Born model was used, where energy is partitioned into long-ranged Coulombic interactions, computed via the Ewald summation technique, and short-ranged atomic pairwise or three-body interactions. The code is unique in that it optimizes the use of crystal symmetry to make structure generation easier and to speed up calculations through the symmetrization of the energy components and their derivatives to second order.

Ionic polarization is treated using the well-known Dick–Overhauser shell model (23) and includes the important coupling between short-range repulsion and ion polarization, which prevents excessive polarization from occurring (i.e., the "polarization catastrophe"). A simple harmonic spring model is used to represent the separation of the shell, which nominally represents the mean position of the valence electron cloud, from the ionic core (nucleus plus core electrons). Within an ion, the shell charge and spring constant combine to determine the overall electronic polarizability. The net ionic (core plus shell) charge may depart from formal charges in order to approximate the effects of partial covalency. GULP also contains a least-squares fitting technique for fitting potential parameters to structural and physical constants, including a "relaxed fitting" method (22).

Total energy minimizations were performed for the zero Kelvin case, which was assumed to correspond to the above experimental data at 298 K, within the uncertainty of the experimental data. Free-energy minimizations were performed at higher temperatures using the quasi-harmonic approximation with analytical free-energy derivatives (24). The ZSISA method (Zero Static Internal Stress Approximation) was used in this work, where only the strains are minimized with respect to the free energy, and the internal degrees of freedom are minimized with respect to the internal energy (25). This approach has been found to be more stable at higher temperatures than total free-energy minimization. Furthermore, the zero point energy was excluded from the free energy in order to equivalence the free-energy and internal-energy calculations at absolute zero, since the potential parameters were derived statically. Phonon sampling was performed using a Monkhorst–Pack shrinking factor of 4 along each crystal axis.

Atomistic simulation is also a tool capable of computing the energetics of isolated defects in extended solids (e.g., 26–28) using the Mott–Littleton approximation (29). However, in the present paper the lattice shrinking and dilation were atomistically simulated using a mean field approximation, which is better suited for high concentrations of detects and their effects on macroscopic properties. This means that the total interatomic potential at a particular site was the sum of potentials for all species (e.g., vacancies and/or substitutions) at that site, each weighted by their partial occupancies. The potential cutoff radii were 10 Å for cation–oxygen interactions and 12 Å for oxygen–oxygen interactions. The energy minimization technique is sensitive to the details of the interatomic potentials, which will be discussed next.

4. INTERATOMIC POTENTIALS

Four sets of potentials were developed and tested for this work, with the objective of simultaneously reproducing (a) the measured unit-cell volumes for oxidized and reduced materials, (b) elastic properties and dielectric constants, (c) the volumetric shrinkage for A-site substitutions, (d) the volumetric expansion upon reduction, and (e) the thermal expansion. In all cases, the potentials were of the Buckingham form, $E\ (\text{eV}) = Ae^{-r/\rho} - C/r^6$, where r is the interatomic separation distance and A, ρ, and C are semiempirical constants. Descriptions of the potentials are given below.

The first set of potentials incorporated the La–O, Cr^{3+}–O, and O–O interactions of Cherry *et al.* (17–20), which were developed for cubic perovskites. It was necessary to fit new Ca–O and Cr^{4+}–O potentials using the oxidized LCC20 data. These potentials treat all the ions as having formal charges, which simplifies interpretations of charge reduction in reducing atmospheres but does not permit partial covalency to be modeled. The potential parameters are shown in Table A1 (see the Appendix) and graphically in Fig. 1. The relative order of the potentials would appear to be inconsistent with expectations based on

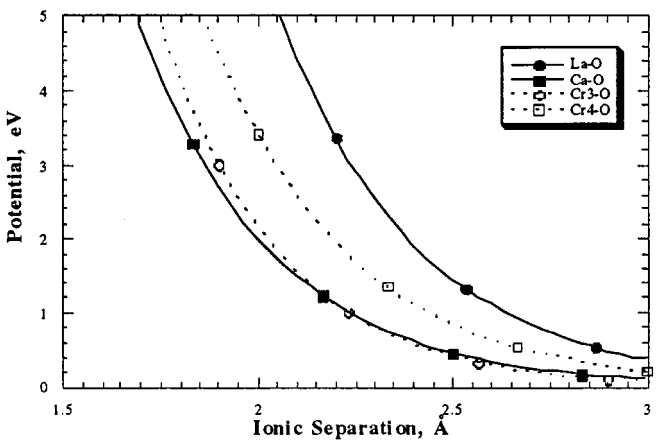

FIG. 1. Supplemented Cherry potentials.

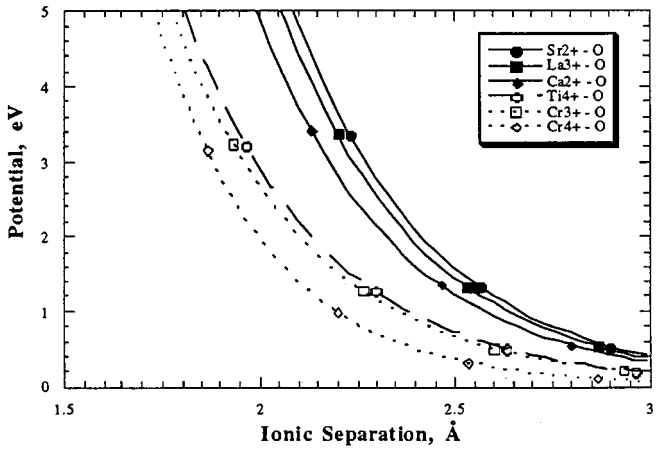

FIG. 2. Potentials developed from a "fundamental perovskite basis set."

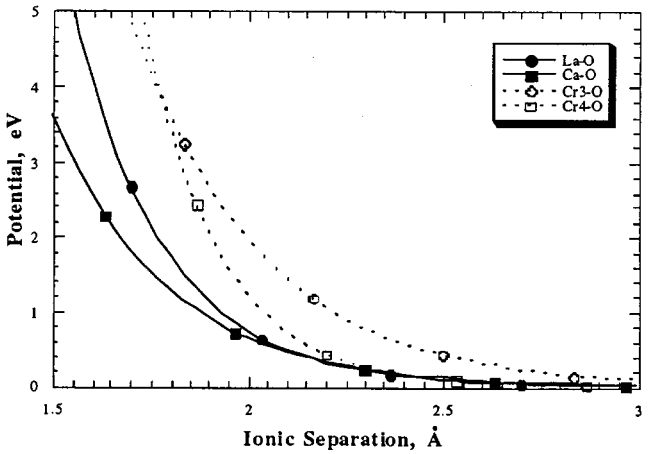

FIG. 4. Partial charge potentials.

Shannon's ionic radii (30, 31), $La > Ca > Cr^{3+} > Cr^{4+}$. This can often occur with empirical potentials because the use of formal charges overestimates the electrostatic attraction, and thus the short-range terms must be adjusted to compensate.

The La–O, Cr^{3+}–O, and O–O interactions of the supplemented Cherry potentials shown above were developed from a "fundamental oxides basis set" (e.g., La_2O_3, Cr_2O_3) to enhance their transferrability to other materials. This practice is often reasonably successful for simpler materials but can be insufficient for more complex materials or for space groups with lower symmetries, such as the present orthorhombic perovskite $La_{1-x}Ca_xCr^{3+}_{1-x+2\delta}Cr^{4+}_{x-2\delta}O_{3-\delta}[V_O^{\cdot\cdot}]_\delta$. In an effort to eliminate deficiencies possibly due to the transition from simpler to more complex materials, we developed a second series of potentials using a fundamental perovskite basis set consisting of $CaTiO_3$, $SrTiO_3$, and $LaCrO_3$. The same O–O potential was employed as above. The end result is shown in Fig. 2. Although these potentials give a good representation of relative ionic radii, the large separation between A-site versus B-site potentials resulted in significant errors in the predicted unit-cell volumes, A-site substitutional shrinkage, and defect-induced expansion. Attempts to decrease the separation between potentials revealed that the volume shrinkages and expansions were much more sensitive to B-site potentials than to A-site potentials. This is consistent with experimental observations.

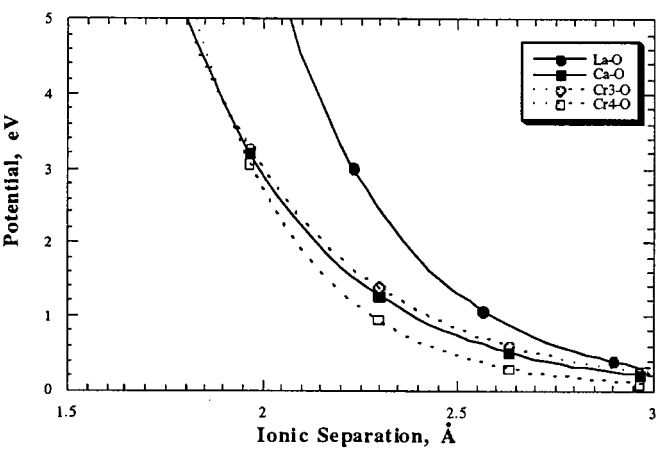

FIG. 3. Modified SOFC-VI potentials.

Although the potentials developed from the perovskite basis set were not successful, observations included the idea that the O–O potential may be too "attractive" for the more complex perovskites in this study. Reductions in the O–O dispersion term (C) caused the dominantly repulsive cation–O potentials to cluster into a slightly smaller group with less separation, but giving unreliable predictions of volumetric change. Several other "less attractive" O–O potentials were explored, including (a) the Bush O–O potential (32), (b) the BKS potential (33), and (c) the Vessal potential (34). The latter two were developed for silicates but were explored here because they incorporate some measure of covalency. None of the potential sets developed with alternate O–O interactions were successful.

The third set of potentials was a modified version from out previous work on $La_{1-x}Sr_xCr_{1-x+2\delta}Cr_{x-2\delta}O_{3-\delta}$

TABLE 1
Percentage Errors in Computed Volumes at 0 K (The Volumes are Given per Formula Unit.)

Material	Vol. (Å^3)	Supp. Cherry	Mod. SOFC-VI	Partial charge
LCC20-ox	57.5187	− 1.19	− 1.40	− 0.08
LCC20-red	57.8444	− 1.26	− 1.55	− 0.18
LCC30-ox	57.2582	− 2.28	− 1.45	− 0.09
LCC30-red	57.8697	− 2.66	− 2.04	− 0.36

TABLE 2
Computed Bulk Modulus, GPa
(The Expected Value is 136 GPa.)

Material	Supp. Cherry	Mod. SOFC-VI	Partial charge
LCC20-ox	230	208	94
LCC20-red	221	172	80
LCC30-ox	232	224	99
LCC30-red	217	173	79

$[V_O^{\cdot\cdot}]_\delta$ (LSC) perovskites (13), where the La–O, Cr^{3+}–O, and Cr^{4+}–O interactions were developed from a basis set of fundamental oxides. A new Ca–O potential was fit to the oxidized LCC20 data, and a dispersion term was added to the La–O potential to improve unit-cell volume predictions. The potentials are shown in Table A2 (see the Appendix) and Fig. 3. Note that the separation between potentials is smaller, indicating that the strong attractiveness of the O–O potentials has been partially overcome. Also, the relative magnitudes are almost consistent with respect to ionic radii, although the Cr–O potentials overlap into the region of the Ca potential. These potentials are reminiscent of the supplemented Cherry potentials shown above. The relative independence of the A-site versus the B-site potentials is visible when Figs. 1 and 2 are compared.

The fourth set of potentials sought to acknowledge that some covalency may exist in the LCC materials. For this purpose, partial charge models were developed as follows. The La–O and Cr^{3+}–O potentials were fit to the $LaCrO_3$ structure and elastic properties by simultaneously varying the core and shell charges, spring constants, and Buckingham parameters. Although the dielectric constant is not physically measurable for these materials, a low value of 5 was also assumed for fitting purposes. Then the Ca–O and Cr^{4+}–O potential parameters, charges, and spring constants were fit to oxidized LCC20 in a similar manner. The resulting parameters are shown in Tables A3 and A4 (in the Appendix), and the potentials are plotted in Fig. 4. In this case, the A-site potentials are lower than those for the B-sites, in contradiction to expectations based on ionic radii. However, as mentioned above, there are often several solutions for complex materials when working with empirical potentials. The partial charge potentials have taken this form partly because some elastic and dielectric constants have been added to the fitting data base. The impact of these additions is shown in the next section. It is noteworthy that the decrease in shell charge of the Cr^{4+} ion for the reduced cases in Table A4 is in agreement with physical expectations. If the total charge in Table A4 can be taken as an indication of the amount of covalency, it could be inferred that bonding in these materials is about 35–40% covalent.

TABLE 3
Computed Static Dielectric Constant ε_{11}
(The Expected Value is <5.)

Material	Supp. Cherry	Mod. SOFC-VI	Partial charge
LCC20-ox	54.5	25.4	6.1
LCC20-red	45.3	30.9	6.5
LCC30-ox	95.1	25.3	6.1
LCC30-red	65.8	32.3	6.4

TABLE 4
Volume Shrinkage at 0 K Caused by A-Site Substitutions (%)

Material	Exp. data	Supp. Cherry	Mod. SOFC-VI	Partial charge
Oxidized	− 1.08	− 1.53	− 0.510	− 0.479
Reduced	− 0.20 (est.)	− 1.32	− 0.440	− 0.138

5. SIMULATION RESULTS

Tables 1–8 show the results of predictions for the bulk modulus and static dielectric constant, volumes per formula unit, A-site substitutional shrinkage, reduction-induced expansion, and thermal expansion for LCC20 and LCC30 from 0 to 1273 K. For convenience, calculations at 0 K are assumed to correspond approximately to experimental data measured at 298 K. This is a reasonable approximation as the thermal expansion coefficient tends to zero at low temperatures. Only the supplemented Cherry, the modified SOFC-VI, and the partial charge potentials were used because the perovskite basis potentials were unsuccessful.

Based on the sum of root mean square (RMS) deviations from the experimental data, it can be seen that the partial charge potentials give the best predictions for volumes, for bulk modulus and static dielectric constant, for the A-site substitutional shrinkage at 0 K, and for the volumetric expansion (CCE) at 0 K. The modified SOFC-VI potentials give the best results for the A-site substitutional shrinkage at 1273 K and for the thermal expansion, while the supplemented Cherry potentials are best for CCE at 1273 K. When the RMS deviations from data are used to provide an overall rating of the potentials, the partial charge and modified SOFC-VI potentials are very close (within about 10%), while the supplemented Cherry potentials are a distant second place. If only high-temperature volumetric

TABLE 5
Volume Shrinkage at 1273 K Caused by A-Site Substitutions (%)

Material	Exp. data	Supp. Cherry	Mod. SOFC-VI	Partial charge
Oxidized	− 1.12	− 1.66	− 0.856	− 0.851
Reduced	− 0.21	− 1.27	− 0.460	+ 0.077

TABLE 6
Volume Expansion at 0 K Caused by Reducing Atomospheres (%)

Material	Estimated	Supp. Cherry	Mod. SOFC-VI	Partial charge
LCC20	0.188	0.165	0.140	0.155
LCC30	0.358	0.235	0.165	0.268

TABLE 8
Thermal Expansion for 0–1273 K (ppm/K) (Measured Value is ~10 ppm/K.)

Material	Supp. Cherry	Mod. SOFC-VI	Partial charge
LCC20-ox	3.61	6.98	0.75
LCC20-red	3.37	9.79	4.50
LCC30-ox	0.48	6.05	− 0.22
LCC30-red	− 0.07	9.74	5.08

changes are considered (Tables 5, 7, and 8), the modified SOFV-VI potentials give the best results. Although the modified SOFC-VI potentials seem most consistent with the ionic radii, their deviations from the structural, elastic, and dielectric properties should be recognized. Last, better thermal expansions (via improved elastic properties) for the oxidized cases could significantly improve the partial charge potentials, since this strongly affects the volumetric changes at high temperatures. It should be noted that the prediction of thermal expansion is a notoriously difficult problem that almost always requires very accurate potentials. Such improved accuracy could be obtained by the generation of a more detailed experimental data base, including: (a) X-ray and neutron diffraction studies to determine lattice constants and atom positions, (b) elastic constants, and (c) measurements of the CTE and CCE. These data are needed at low and high temperatures and under oxidizing and reducing conditions. Elastic constants are particularly important because they determine the curvatures of the potentials.

6. SUMMARY AND CONCLUSIONS

Four sets of interatomic potentials were developed and tested in an effort to develop predictive simulation models that could eventually reduce the expense of developing solid oxide fuel cell interconnect materials. Two potentials sets were developed by fitting to basis sets composed of simple oxides (the "supplemented Cherry" and "modified SOFC-VI" potentials), one using a perovskite basis set and one fitting to the LCC data itself. Efforts using the perovskite basis set were unsuccessful. The fourth potential set employed partial charges to represent covalent contributions to bonding in the LCC materials.

The objectives were to reproduce the available data for the structures, elastic properties, volumetric shrinkage due to substitutions on the A-site, defect-induced volumetric expansion caused by reducing atmospheres, and thermal expansion. Although many of these objectives were met, it is important to realize that all were not met simultaneously by any single set of potentials. The partial charge potentials gave the best results for the structures, properties, and volumetric shrinkage/expansion at low temperatures, at the expense of losing the physical connection with ionic radii. Potentials developed from a simple oxide basis set gave the best results for high-temperature shrinkage/expansion and thermal expansion, while maintaining a closer relationship to ionic radii. These results would seem to indicate that the material may be too complex, or the data base too sparse, to model the full range of properties and performance with just one set of empirical potentials. However, combinations of the partial charge and simple oxide basis potentials may eliminate this difficulty in future work, if additional experimental data become available for fitting the potentials.

TABLE 7
Volume Expansion at 1273 K Caused by Reducing Atmospheres (%)

Material	Exp. data	Supp. Cherry	Mod. SOFC-VI	Partial charge
LCC20	0.188	0.158	0.491	0.633
LCC30	0.358	0.288	0.627	0.949

APPENDIX A: INTERATOMIC POTENTIAL PARAMETERS

TABLE A1
Buckingham Parameters for Supplemented Cherry Potentials

Ion pair	A (eV)	ρ (Å)	C (eV Å^6)	$Y(\|e\|)$	K_s (eV Å^{-2})
La^{3+}–O	1545.2100	0.3590	0.00	− 0.250	145.00
Ca^{2+}–O	757.9020	0.3370	0.00	1.526	10.41
Cr^{3+}–O	1690.9000	0.3010	0.00	0.950	67.00
Cr^{4+}–O	905.8570	0.3584	0.00	3.970	67.00
O–O	22764.3000	0.1490	43.00	− 2.240	42.00

TABLE A2
Buckingham Parameters for modified SOFC-VI Potentials

Ion pair	A (eV)	ρ (Å)	C (eV Å^6)	$Y(\|e\|)$	K_s (eV Å^{-2})
La^{3+}–O	2983.9880	0.3236	25.00	− 0.250	145.00
Ca^{2+}–O	766.9862	0.3592	0.00	1.526	11.41
Cr^{3+}–O	522.7250	0.3876	0.00	2.995	67.00
Cr^{4+}–O	3448.2306	0.2800	0.00	3.970	67.00
O–O	22764.3000	0.1490	43.00	− 2.240	42.00

TABLE A3
Buckingham Parameters for Partial Charge Potentials

Ion pair	A (eV)	ρ (Å)	C (eV Å^6)
La^{3+}–O	3729.2336	0.2347	0.00
Ca^{2+}–O	634.7258	0.2903	0.00
Cr^{3+}–O	874.5414	0.3278	0.00
Cr^{4+}–O	39202.4160	0.1926	0.00
O–O	22764.300	0.1490	43.00

TABLE A4
Core/Shell Charges (|e|) and Spring Constants (eV Å^{-2}) for Partial Charge Potentials

Parameter	LCC20-ox	LCC20-red	LCC30-ox	LCC30-red
La-core	0.2180	0.2375	0.2293	0.2211
La-shell	0.5500	0.5835	0.6525	0.6654
La-spring	258.02	259.52	256.09	246.21
Ca-core	− 0.2690	− 0.2689	− 0.2668	− 0.0071
Ca-shell	0.9930	0.7809	0.8432	0.5726
Ca-spring	65.40	66.81	65.48	103.02
Cr3-core	0.0050	0.0050	0.0050	0.0050
Cr3-shell	2.9950	2.9950	2.9950	2.9950
Cr3-spring	67.00	67.00	67.00	67.00
Cr4-core	0.0290	0.0290	0.0290	0.0290
Cr4-shell	2.9625	0.4234	2.9800	0.4874
Cr4-spring	67.18	67.18	67.18	67.18
O-core	− 0.0120	− 0.0120	− 0.0129	− 0.0129
O-shell	− 1.2405	− 1.2405	− 1.2514	− 1.2514
O1-spring	270.28	267.98	270.77	232.90
O2-spring	197.35	194.52	203.52	226.19

ACKNOWLEDGMENTS

This work was sponsored by the U.S. Department of Energy's Morgantown Energy Technology Center under contract 22407. Pacific Northwest National Laboratory is operated for the U.S. Department of Energy by the Battelle Memorial Institute under contract DE-AC06-76RLO 1830. J. D. G. thanks the Royal Society for a University Research Fellowship and the EPSRC for provision of computing facilities.

REFERENCES

1. J. Mizusaki, S. Yamauchi, K. Fueki, and A. Ishikawa, *Solid State Ionics* **12,** 119 (1984).
2. D. P. Karim and A. T. Aldred, *Phys. Rev. B* **20**(6), 2255–2263 (1979).
3. T. R. Armstrong, J. W. Stevenson, L. R. Pederson, and P. E. Raney, *J. Electrochem. Soc.* **143**(9), 2919 (1996).
4. P. H. Larsen, P. V. Hendriksen, and M. Mogensen, *in* "Proceedings of the Third European Solid Oxide Fuel Cell Forum" (P. Stevens, Ed.), p. 181. Nantes, France, 1998.
5. H. Yokokawa, T. Horita, N. Sakai, B. van Hassel, T. Kawada, and M. Dokiya, *in* "Solid Oxide Fuel Cells III" (S. C. Singhal and H. Iwahara, Eds.), PV 93-4, p. 364. The Electrochemical Society Proceeding Series, Pennington, NJ, 1993.
6. I. Yasuda and T. Hikita, *in* "Solid Oxide Fuel Cells II" (F. Grosz, P. Zegers, S. C. Singhal, and O. Yamamoto, Eds.), EUR 13564EN, p. 654. Commission of the European Communities, Luxembourg, 1991.
7. J. Hartvigsen, S. Elangovan, C. Milliken, A. Khandkar, M. Ostenstad, and T. Sira, *in* "Third International Symposium on Ionic and Mixed Conducting Ceramics" (W. Gopel, A. Khandkar, M. Mogensen, T. A. Ramanarayanan, H. L. Tuller, and W. L. Worrell, Eds.). The Electrochemical Society Proceedings Series, Pennington, NJ, 1997.
8. S. Srilomsak, D. P. Schilling, and H. U. Anderson, *in* "Solid Oxide Fuel Cells I" (S. C. Singhal, Ed.), PV 89-11, p. 129. The Electrochemical Society Proceeding Series, Pennington, NJ, 1989.
9. T. R. Armstrong, J. W. Stevenson, L. R. Pederson, and P. E. Raney, *in* "Solid Oxide Fuel Cells IV" (M. Dokiya, O. Yamamoto, H. Tagawa, and S. C. Singhal, Eds.), PV 95-1, p. 944. The Electrochemical Society Proceedings Series, Pennington, NJ, 1995.
10. P. V. Hendriksen, J. D. Carter, and M. Mogensen, *in* "Solid Oxide Fuel Cells IV" (M. Dokiya, O. Yamamoto, H. Tagawa, and S. C. Singhal, Eds.), PV 95-1, p. 934. The Electrochemical Society Proceedings Series, Pennington, NJ, 1995.
11. P. H. Larsen, P. V. Hendriksen, and M. Mogensen, *J. Thermal Anal.* **49,** 1263–1275 (1997).
12. T. R. Armstrong, J. W. Stevenson, D. E. McCready, S. W. Paulik, and P. E. Rainey, *Solid State Ionics* **92,** 213–223 (1996).
13. R. E. Williford and T. R. Armstrong, *in* "Solid Oxide Fuel Cells VI, Honolulu, October, 1999" (S. C. Singhal and M. Dokiya, Eds.), The Electrochemical Society Proceedings Series, Pennington, NJ, 1999.
14. T. R. Armstrong, J. W. Stevenson, K. Hasinska, and D. E. McCready, *J. Electrochem. Soc.* **145**(12), 4282 (1998).
15. C. P. Khattak and D. E. Cox, *Mater. Res. Bull.* **12,** 43 (1977).
16. W. Paulik, S. Baskaran, and T. R. Armstrong, *J. Mater. Sci.* **33,** 2398 (1998).
17. M. Cherry, M. S. Islam, J. D. Gale, and C. R. A. Catlow, *J. Phys. Chem.* **99,** 14614 (1995).
18. M. S. Islam, M. Cherry, and C. R. A. Catlow, *J. Solid State Chem.* **124,** 230 (1996).
19. M. S. Islam, M. Cherry, and L. J. Winch, *J. Chem. Soc. Faraday Trans.* **92**(3), 479 (1996).
20. M. S. Khan, M. S. Islam, and D. R. Bates, *J. Phys. Chem. B* **102,** 3099 (1998).
21. J. D. Gale, *J. Chem. Soc. Faraday Trans.* **93,** 629 (1997).
22. J. D. Gale, *Phil. Mag. B* **73,** 3 (1996).
23. B. G. Dick and A. W. Overhauser, *Phys. Rev.* **112,** 90 (1958).
24. J. D. Gale, *J. Phys. Chem. B* **102,** 5423 (1998).
25. N. L. Allen, T. H. K. Barron, and J. A. O. Bruno, *J. Chem. Phys.* **105,** 8300 (1996).
26. R. E. Williford, R. Devanathan, W. J. Weber, and A. N. Cormack, *J. Nucl. Mater.* **273,** 164 (1999).
27. R. E. Williford, W. J. Weber, R. Devanathan, and J. D. Gale, *J. Electroceram.* in press.
28. R. E. Williford and W. J. Weber, *J. Am. Ceram. Soc.* **82**(12), 1999.
29. N. F. Mott and M. J. Littleton, *Trans. Faraday Soc.* **34,** 485 (1938).
30. R. D. Shannon, *J. Appl. Phys.* **73**(1), 348 (1993).
31. R. D. Shannon and C. T. Prewitt, *Acta Crystallogr. B* **25,** 925 (1969).
32. T. S. Bush, J. D. Gale, C. R. A. Catlow, and P. D. Battle, *J. Mater. Chem.* **4**(6), 831 (1994).
33. G. J. Kramer, N. P. Farragher, B. W. H. van Beest, and R. A. van Santen, *Phys. Rev. B* **43**(6), 5068 (1991).
34. B. Vessal, *J. Non-Cryst. Solids* **177,** 103 (1994).